CHARACTERIZATION OF CELL SHAPE AND DEFORMATION IN 3D USING SPHERICAL HARMONICS

Christel Ducroz, Jean-Christophe Olivo-Marin, Alexandre Dufour

Institut Pasteur, Quantitative Image Analysis Unit, F-75015 Paris, France
CNRS URA 2582, F-75015 Paris, France

ABSTRACT

Understanding the mechanisms involved in cell deformation and motility is of major interest in numerous areas of life sciences. Precise quantification of cell shape requires robust shape description tools to be amenable to subsequent analysis and classification. The main difficulty lies in the great variability of cell shapes within so-called "homogeneous" populations. While basic shape descriptors fail to provide sufficient information and lack robustness to small shape variabilities, here we investigate the use of the Spherical Harmonics transform to efficiently extract and quantify cell shape and deformation. Using real 3D+t biological imaging data sets, we show that this tool allows to precisely characterize the cell shape both in a static and a dynamic manner, allowing to extract a wide range of qualitative and quantitative parameters, such as outliers individuals, redundant shape configurations and spatiotemporal deformation patterns.

Index Terms— Spherical Harmonics, Shape analysis, Pattern recognition

1. INTRODUCTION

Cell deformation is central to several fundamental biological processes, many of which have important medical implications. For instance, cells of a developing embryo migrate to distant locations, where they specialize in shape and in function on the onset of organ morphogenesis. More generally, cells and unicellular organisms characterized by amoeboid motion exhibit an ordered cycle of complex shape changes in order to generate movement [1, 2]. Understanding the mechanisms and factors underlying cellular shape is thus a crucial aspect in cell biology, and calls for shape quantification tools able to efficiently describe and further discriminate the variety of shape configurations. To this end, a wealth of generic shape descriptors have been proposed in the literature over the past decades. Simple descriptors include basic measures such as size or sphericity, while morphological descriptors exploit a voxelized representation of the object to compute skeletons and other geodesic features from the object. Such descriptors are simple and intuitive, yet they only provide an approximate description of the shape, moreover they are particularly sensitive to small shape variability. To overcome these limitations, more advanced mathematical descriptors based on frequency analysis have been developed, and aim to represent the surface of a given object as a combination of basis mathematical functions. In this work we focus on the SPherical HARMonics transform (SPHARM) which has received extensive attention over the past years in the biomedical imaging field for various tasks including shape modeling and comparison [3, 4]. The SPHARM transform considers any closed shape as a function of the unit sphere, and simplifies this function into a unique set of coefficients, facilitating subsequent shape characterization and classification tasks. They are particularly well suited for shape sets exhibiting important shape variability such as living cells, and offer interesting properties such as position and orientation invariance.

Hereafter we describe a novel application of the SPHARM transform to characterize and study the shape and deformation of living cells observed in 3D time-lapse fluorescence microscopy. Section 2 describes the main steps of the SPHARM analysis, from surface extraction to the actual SPHARM transform. Section 3 then presents analysis results on biological data. Finally, section 4 concludes the paper.

2. SPHERICAL HARMONICS ANALYSIS

2.1. Surface extraction and mapping

In order to perform spherical harmonic analysis of the cell shape, its surface yet has to be extracted from the image data, and represented as a spherical signal. The surface extraction step is achieved using the 3D Active Mesh segmentation method previously published in [5]. This method has the advantage of extracting each cell surface as a 3D triangular mesh, making it directly suitable for spherical mesh parameterization techniques. In this work we focus more specifically on bijective mapping techniques, in order to ensure uniqueness of the analysis and reconstruction of the original surface from its spherical projection.

A number of surface parameterization methods have been proposed in the past years [6]. While early approaches relied on a voxel-based representation of the object surface [7], more recent techniques have allowed to map arbitrary triangular meshes, e.g. [8, 9]. Here we use the CALD framework [9], where the mapping process starts by an initialization step whereby a North and a South pole are chosen on the surface, such that they have the greatest distance to the principal shape axis. The algorithm then performs an iterative mapping on the sphere while controlling area and length distortions simultaneously. This is done by alternating between a local and a global smoothing. Local smoothing minimizes the area distortion by moving each vertex such that all triangles in the immediate neighborhood have equal area. Global smoothing equalizes the area distortion over the entire mesh by rotating the most distorted vertex towards the North Pole. This step rearranges the parameter space so that every spherical region is converted to a new region with same area as the corresponding region on the object surface. The local-global smoothing process is then repeated until convergence. An illustration of the surface mapping is given in Fig. 1. The computation of the spherical parameterization and of the spherical harmonic transform are made thanks to the SPHARM-MAT toolbox.

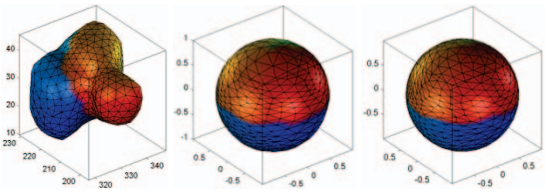


Fig. 1. Spherical parametrization process. The original mesh (left) is first mapped to the sphere (middle), then the mapping is re-adjusted to minimize local and global distortions (right).

2.2. Spherical Harmonics Transform

We start below by recalling the main principles of the SPHARM transform for functions defined on the unit sphere, and then discuss several of its properties for the purpose of cell shape description.

2.2.1. *Method*

Spherical harmonic analysis is generally considered as the extension of Fourier analysis on the unit sphere. In the same way that vectors can be described through projections onto each axis (using scalar products), expansion coefficients (scalar product between functions) can be used to describe functions. On the unit sphere, an orthonormal basis for the Hilbert space of square-integrable function is given by the spherical harmonics:

$$Y_l^m(\theta,\varphi) = k_{l,m} P_l^m(\cos\theta) e^{im\varphi},$$

where l and m are respectively the degree and order of the harmonic, $k_{l,m}$ is the expansion coefficient and P_l^m is the associated Legendre polynomial. Using this basis, any spherical scalar function $f(\theta,\varphi)$ can be expanded as follows (cf. Fig. 2):

$$f(\theta,\varphi) = \sum_{l=0}^{\infty} \sum_{m=-l}^{l} \hat{f}(l,m) Y_l^m(\theta,\varphi),$$

where $\hat{f}(l,m)$ is the (l,m) harmonic coefficient, given by:

$$\hat{f}(l,m) = k_{l,m} \int_0^{\pi} \int_0^{2\pi} e^{-im\varphi} f(\theta,\varphi) P_l^m(\cos\theta) \sin\theta \, d\varphi \, d\theta.$$

The coefficients $\hat{f}(l,m)$ are unique and can thus describe any arbitrary shape. The spectral decomposition of the input signal is then straightforward: lower degrees (i.e. l) correspond to low frequencies and hence describe the global shape of the object, while higher degrees describe the details of the surface, as illustrated in Fig. 3.

Higher dimensional (non-scalar) spherical functions can also be expanded using spherical harmonics, by expanding each component of the function independently. Here we perform the spherical harmonic transform on a surface defined in the Cartesian space (x,y,z) and parametrized into a spherical signal defined in the polar system (θ,φ) as $\mathbf{v}(\theta,\varphi) = (x(\theta,\varphi)\ y(\theta,\varphi)\ z(\theta,\varphi))^\top$. As (θ,φ) runs over the sphere, $\mathbf{v}(\theta,\varphi)$ runs over the object surface. By applying the SPHARM transform to each component of $\mathbf{v}(\theta,\varphi)$ independently, we obtain coefficients with three components.

2.2.2. *Rotational invariance*

An intrinsic property of the SPHARM transform is that any arbitrary rotation in the parameter space corresponds to a rotation in the object space. This property allows to compute descriptors that

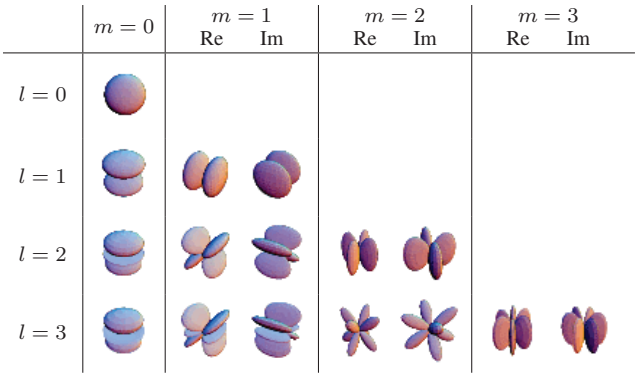


Fig. 2. First four degrees of the SPHARM basis. Adapted from [10]

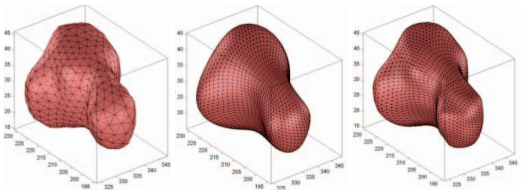


Fig. 3. SPHARM reconstruction of an arbitrary mesh (left) with a maximum level $l_{\text{MAX}} = 5$ (middle) and $l_{\text{MAX}} = 11$ (right). Higher levels reconstruct the finer details of the surface.

are rotationally invariant [11], thus allowing generalized shape comparison and classification. Hence, by expanding each component of the spherical signal $\mathbf{v}(\theta,\varphi)$, we obtain three set of coefficients C_x, C_y, C_z, and compute a rotationally invariant descriptor as follows: $\hat{C} = \sqrt{(C_x^2 + C_y^2 + C_z^2)}$.

2.2.3. *Coefficients interpretation*

Similarly to a Fourier expansion, SPHARM polynomials of increasing degree l describe information at finer scales. Hence, each coefficient of the expansion retains an information corresponding to a particular spatial frequency. The first coefficients are illustrated in Fig. 2, where the coefficient $(l = 0, m = 0)$ represents the mean radius of the cell. As the order increases, the template shape in the basis captures higher frequency information and thus more complex shapes, such as the *eight* $(l = 1)$, the *elongated cross* $(l = 2)$, the *butterfly* $(l = 3, m = \pm 1)$, the *star* $(l = 3, m = \pm 2)$ and the *fan* $(l = 3, m = \pm 3)$. Starting from $l = 1$, the basis shapes capture asymmetric information, which is particularly needed to study cell deformation, as we shall discuss below.

3. EXPERIMENTAL RESULTS

Here we present a practical application of SPHARM analysis to study the deformation of *Entamoeba histolytica* unicellular parasites, the causative agent of the amoebiasis disease. These parasites are characterized by an amoeboid motility, i.e., the formation of asymmetric protuberances (so-called *blebs*) which allow the parasite to scan its environment and eventually induce motion [12]. We briefly describe below the experimental setup and then present SPHARM analysis results.

3.1. Data acquisition and surface extraction

Parasites are labeled using fluorescent dye and embedded into a 3D collagen matrix, letting them deform and move freely by degrading and carving the collagen using specific enzymes. Images are acquired on a Nipkov-disk confocal 3D microscope equipped with a $25\times$ (NA 0.8) oil-immersed objective and a 12-bit Andor camera, yielding images of digital size 1024×1024 pixels and plane resolution 0.327×0.327 μm (i.e. the field of view is 335×335 μm wide, allowing to observe up to 15 parasites simultaneously). Each 3D stack is obtained by acquiring 32 consecutive planes along the depth axis with an inter-plane distance of 3 μm, resulting in a depth resolution about ten times lower than the axial resolution. Finally, 3D time-lapse sequences are obtained by acquiring 90 of these 3D stacks with an interval of 10 seconds between stacks (i.e. the total observation time per experiment is 15 minutes), yielding a typical data size of 5.625 GigaBytes per 4D sequence. A total of 52 videos were acquired, and 274 cells were observed and automatically tracked over time using the Active Mesh framework (cf. [5] for further details).

3.2. Detection of outliers

Outlier cells are those considered as not suitable for correct shape and deformation analysis. We distinguish here two types of outliers: incomplete surfaces and dead cells. The former describe cells lying across the boundary of the acquisition volume, and thus only partially extracted by the segmentation method (cf. fig. 4). This resulting shape can be easily detected within the coefficients $l = 1, m = \pm 1$ and hence removed from subsequent analysis.

Dead cells are easily characterized by their lack of deformation. They can thus be easily extracted by computing the cumulative variance of all SPHARM coefficients over time and extracting the cells with values close to zero (cf. fig. 5).

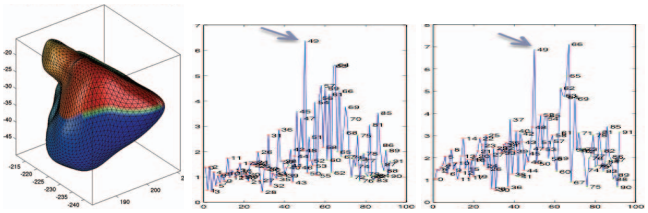


Fig. 4. Detection of cells on the edge of the acquisition field: the cell surface (left) has been detected in the coefficients $l = 2, m = \pm 1$ (Re) (middle) and $l = 2, m = \pm 1$ (Im) (right), at frame 49 (gray arrow).

3.3. Temporal pattern recognition

Temporal analysis has many more applications than outliers detection. In [13], we used SPHARM analysis to detect major deformation phases based on the evolution of all coefficients over time. Here we push this idea further by detecting temporal events of interest, such as the formation of blebs as well as patterns of deformation.

3.3.1. Amoeboid motion

Amoeboid motion is characterized by the formation of a bleb on the side of the cell that may in some cases adhere to the substrate, followed by a global deformation of the amoeba in the direction of the bleb. Since blebs are small with respect to the cell size, they can be detected in the higher degree coefficients, carrying more asymmetric shape information, namely $l = 2, m = \pm 1$ (cf. fig. 6-b).

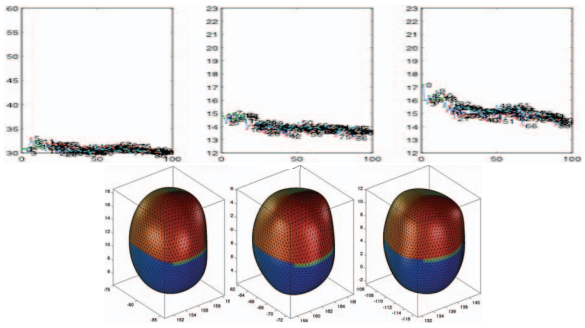
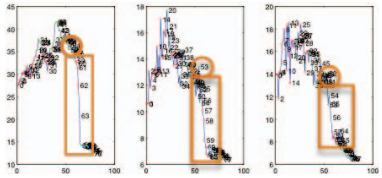
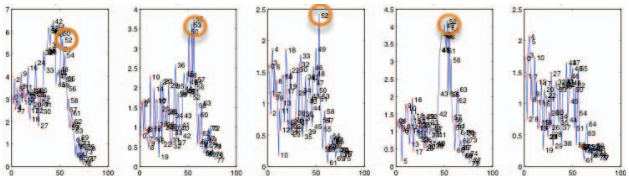


Fig. 5. Detection of a dead cell. Top: Evolution of the $l = 1$ coefficients over shows a temporal variance close to 0. Bottom]: As expected, the corresponding cell shape at the beginning, middle and end of the sequence is almost identical.

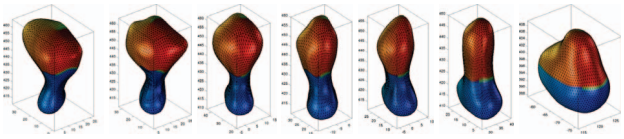
Interestingly, the deformation pattern itself can also be detected with the SPHARM coefficients, and is strikingly highly conserved throughout the observed population (cf fig. 6-a). Indeed, right after a bleb has been detected in the higher degrees, a rapid decrease is observed in all coefficients including those at lower degrees, indicating an important conformation change towards a more spherical shape. Note that this pattern was observed for more than 70 amoebas.



(a) $l = 1$ $(m = 0, m \pm 1\ Re, m \pm 1\ Im)$



(b) $l = 2$ $(m = 0, m \pm 1\ Re, m \pm 1\ Im, m \pm 2\ Re, m \pm 2\ Im)$



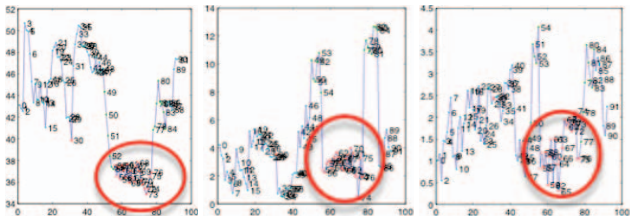
(c) shape evolution after the bleb formation

Fig. 6. Bleb-induced deformation. After a bleb is detected (orange circles), all coefficients decrease rapidly (orange boxes), yielding a global cell deformation towards a simpler (spherical) shape.

3.3.2. Other temporal patterns

With the ability to automatically extract known deformation patterns from the SPHARM coefficients, we investigated whether unknown patterns could also be highlighted, thus proving the efficiency and relevance of the proposed approach. Since the cumulative variance of the coefficients allowed to detect dead cells, we reduced the accumulation window and managed to highlight a particular deformation

pattern which we named "stop'n'go" motion, whereby the cell deforms, then stops for a while before resuming its deformation (cf. Fig. 7). This phenomenon applies to all coefficients and was observed on as many as 50 different cells in the data set. Further biological investigation is currently pursued to interpret such phenomenon, that had never been clearly observed using previous approaches.

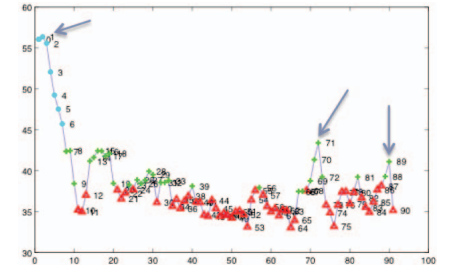


(a) $l = 1, m = 0$ (b) $l = 2, m = 0$ (c) $l = 3, m = 0$

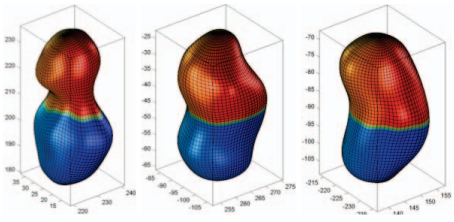
Fig. 7. Evolution of three coefficients over time. The circles highlight periods of pause during the deformation.

4. CONCLUSION

We have presented a novel application of the spherical harmonics transform to describe and analyze the shape and deformation of cells over time. We have shown that this approach can be used to extract numerous static and dynamic patterns over time with great robustness. Among these patterns, we were able to recognize known deformations profiles such as amoeboid motion. But more interestingly, novel deformation patterns could be detected using the proposed method and couldn't be recognized by simple visual assessment, suggesting that the proposed tool can provide novel insight into numerous morpho-dynamic processes at the cell level.

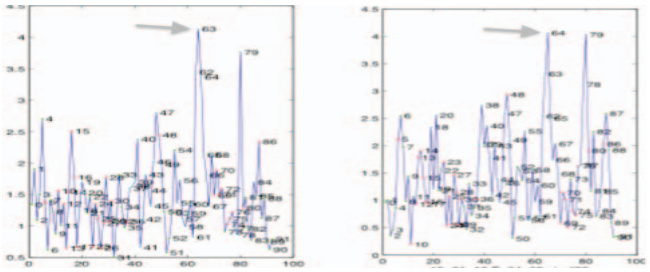


(a) $l = 1, m = 0$ over time

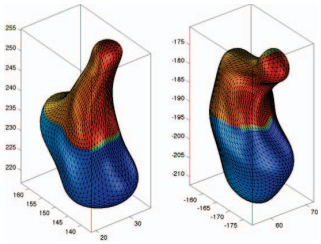


(b) cell shapes (top arrows)

Fig. 8. Interpretation of the $l = 1, m = 0$ coefficient: the graph represents the evolution of the coefficient over time for one given cell and the three shapes correspond to the three peaks in the graph (indicated by gray arrows).



(a) $l = 2, m = \pm 1$ (left: real, right: imaginary)



(b) cell shapes (top arrows)

Fig. 9. Interpretation of the $l = 2, m = 1$ coefficient: the two graphs represent the evolution of the real and imaginary parts of the coefficients over time, while the two shapes correspond to the two peaks in the graph.

5. REFERENCES

[1] R. Ananthakrishnan, and A. Ehrlicher, "The forces behind cell movement", *Int. J Biol Sci.*, vol. 3, no. 5, 2007, pp. 303-317.

[2] R. McBeath, D.M. Pirone, C.M. Nelson, K. Bhadriraju, and C.S. Chen, Cell shape, cytoskeletal tension, and RhoA regulate stem cell lineage commitment", *Develop. Cell*, vol. 6, no. 4, 2004, pp. 483-495.

[3] D.W. Ritchie, and G.J.L. Kemp, "Fast Computation, Rotation and Comparison of Low Resolution Spherical Harmonic Molecular Surfaces", *J. Comp. Chemistry*, vol. 20, no. 4, 1999, pp. 383-395.

[4] K. Khairy, J. Foo, and J. Howard, "Shapes of Red Blood Cells: Comparison of 3D Confocal Images with the Bilayer-couple Model", *Cell. and Mol. Bioeng.*, vol. 1, 2008, pp. 173-181.

[5] A. Dufour, R. Thibeaux, E. Labruyère, N. Guillén, and J.-C. Olivo-Marin, "3D Active Meshes: fast discrete deformable models for cell tracking in 3D time-lapse microscopy", *IEEE Trans. Image Proc.*, vol. 20, no. 7, 2011, pp. 1925-1937.

[6] M. Floater, and K. Hormann, "Surface parameterizations: a tutorial and survey", *in Advances in Multiresolution for Geometric Modelling*, N.A. Dodgson, M.S. Floater and M. A. Sabin, Eds., Springer-Verlag, 2004, pp. 157-186.

[7] C. Brechbuhler, G. Gerig, and O. Kubler, "Parametrization of Closed Surfaces for 3-D Shape Description", *Computer Vision and Image Understanding*, vol. 61, no. 2, 1995, pp. 154-170.

[8] X. Gu, and Y. Wang, and T.F. Chan, and P.M. Thompson, and S.T. Yau, "Genus zero surface conformal mapping and its application to brain surface mapping", *IEEE Trans. Med. Imag.*, vol. 23, no. 8, 2004, pp. 949-958.

[9] L. Shen, and F. Makedon, "Spherical mapping for processing of 3D closed surfaces", *Image and Vision Computing*, vol. 24, no. 7, 2006, pp. 743-761.

[10] E.W. Weisstein "Spherical Harmonic" from MathWorld–A Wolfram Web Resource. http://mathworld.wolfram.com/SphericalHarmonic.html

[11] M. Kazhdan, and T. Funkhouser, and S. Rusinkiewicz, "Rotation invariant spherical harmonic representation of 3D shape descriptors", *Proc. Eurographics Symp. on Geometry Proc.*, 2003.

[12] B. Maugis, J.Brugues, P. Nassoy, N. Guillen, P. Sens and F. Amblard, "Dynamic instability of the intracellular pressure drives bleb-based motility", *J. Cell Sci.*, no. 123, 2010, pp. 3884-3892.

[13] C. Ducroz, J.-C. Olivo-Marin and A. Dufour, "Spherical Harmonics based extraction and annotation of cell shape in 3D time-lapse microscopy sequences", *Proc. EMBC*, Boston, 2011.